DOI:
10.1111/jop.12663

Document Version
Peer reviewed version

Epithelial disruptions, but not immune cell invasion, induced secretory dysfunction following innate immune activation in a novel model of acute salivary gland injury.

Abeer Shaalan[1*], Guy Carpenter[1] and Gordon Proctor[1]

[1] Mucosal and Salivary Biology Division, Dental Institute, King's College London, Guy's Hospital, Floor 17, Tower Wing, London SE1 9RT, UK

*Corresponding author: abeer.shaalan@kcl.ac.uk.

Running title: Salivary gland dysfunction

Keywords: innate; salivary glands; AQP-5; M3R; TMEM16A; NKCC1; M3R

Abstract

Background

Salivary gland (SG) injurious agents are all translated into loss of salivation (xerostomia). An association has been established between activation of innate immunity and salivary gland injury and dysfunction. However, it remains unclear how the secretory epithelia respond by halting saliva production.

Methods

C57BL/6 submandibular glands (SMGs) were acutely challenged using a single dose of the innate immune stimulant: polyinosinic-polycytidylic acid (poly (I:C)). Secretory capacity of the infected SMGs was substantiated by assessing the flow rate in response to pilocarpine stimulation. Depletion of the acute inflammatory cells was achieved by pre-treating mice with RB6-8C5 depletion antibody. Flow cytometry, histology and immunohistochemistry were conducted to verify the immune cell depletion. Epithelial expression of saliva-driving molecules: muscarinic 3 receptor (M3R), aquaporin 5 water channel (AQP5), Na-K- CL-Cotransporter 1 (NKCC1) and transmembrane member 16A (TMEM16A), were characterized using RT-qPCR and immunohistochemistry. Tight junction (TJ) protein; zonula occludens (ZO-1) and basement membrane (BM) protein; laminin were assessed by immunohistochemistry.

Results

Innate immune challenge prompted dysfunction in the exocrine salivary glands (SGs). Dysregulated gene and protein expression of molecules that drive saliva secretion was substantiated. Aberrant expression of TJ and BM proteins followed innate immune activation. Hyposalivation in the current model was independent of myeloperoxidase (MPO)-positive, acute inflammatory cells.

Conclusions

In the present study, we developed a novel injury model of the SGs, featuring acute secretory dysfunction and immediate structural disruptions. Our results ruled out the injurious role of aggressively infiltrating inflammatory cells.

Introduction

Saliva performs a number of important functions that are essential for the maintenance of oral health [1]. Dysfunction of the SG leads to oral dryness (xerostomia), which raises the risk of gingivitis, tooth decay, and mouth infections. A comprehensive understanding of the mechanism(s) which interfere with the ability of these exocrine glands to secrete will only be derived from a sound knowledge of the pathological changes that can occur during early stages of acute injury. In the current study, a novel acute SG injury model is introduced and based on direct injection of the potent innate immune stimulant poly (I:C) [2], into the SMGs. Our work focused on characterizing the initial: functional, immune, structural and molecular consequences of challenging the SMG innate immune system.

In various models, poly (I:C) prompted an acute inflammatory response, featuring the migration and activation of innate immune cells, principally neutrophils and monocytes [3]. Since the most common salivary gland diseases are inflammatory in origin and share salivary hypofunction [4], acute exposure of the SGs to inflammatory cells (mainly neutrophils and monocytes) and the potential therapeutic effect of their specific depletion, will be elucidated.

Briefly, saliva fluid secretion is initiated in response to the action of the parasympathetic postganglionic transmitter; acetylcholine on the acinar M3 muscarinic receptors (M3R) [5] and involves increase intracellular calcium $[Ca^{2+}]_i$ and ion transport, which activates the apical chloride (Cl-) channel; TMEM16A [6]. TMEM16A activation will release cytosolic Cl-, that has been accumulated in the resting acinar cells above electrochemical equilibrium, via the sodium potassium chloride co-transporter (NKCC1) [7]. Cl- discharge into the central acinar lumen by TMEM16A, will be followed by sodium movement via a paracellular course through the TJs [8]. Typically, the transcellular accumulation of NaCl ions in the acinar lumen will result in the obligatory osmotic water flow [9]. Although water can cross the membrane bilayer, water flow in secretory cells is facilitated by the water channels; aquaporins (AQPs). While the integrity of the formerly mentioned functional determinants is indispensable in the saliva secretion process, they have not been previously assessed, following engagement of the innate immune system.

An association has been established between innate immune activation and diseases of the salivary glands [10, 11]. However, the initial events which follow challenging the exocrine immune system have not been previously demonstrated. The aim of the current study was to: (i) develop a model of acute salivary gland dysfunction, (ii) substantiate invasion of acute inflammatory cells following local exposure to poly (I:C) and (iii) delineate the potential injurious impact of these cells on the secretory machinery. (iv) The effect of challenging the SMG innate immunity on key, water-driving, receptors, channels and ion transporters will be explored. In addition, (v) the expression of TJ and BM proteins will be characterized.

Materials and Method

Mice

Female C57BL/6 mice weighing 18-21 grams (Harlan Labs Ltd., Loughborough, UK) and aged 10-12 weeks were housed in a temperature-controlled environment under a 12 h light–dark cycle, with free access to food and water. All procedures were approved by the local ethics committee and performed under general anaesthesia under a Home Office license.

Poly (I:C) injury model

Poly (I:C) (P1530-25MG, Sigma-Aldrich) was diluted in saline (4mg/ml). Towards visualised injection, poly (I:C) was pre-mixed with Trypan blue (T8154-100ML-Sigma- Aldrich) (Fig. 1A). Eighty micrograms of poly (I:C) in 20 µls were loaded into a 0.3 ml syringe (6134900, VWR International), attached to a glass cannula (Supelco, 25715, PA- USA). For recovery experiments, mice were anaesthetised intraperitoneally (i.p.) with 0.1 ml of combined 5 mg Ketamine/1 mg Xylazine. Under a stereomicroscope, the glass cannula was inserted into Wharton's duct and poly (I:C) was injected slowly and constantly into the left SMG (Fig. 1B, C and D). The same volume of the vehicle was delivered to the right SMG as a contralateral negative control.

Assessment of SMG secretory function

Animals were anaesthetized with 150 µl of Pentobarbital Sodium (Euthatal, Merial) 1 mg/ml (i.p.), followed by endotracheal intubation. SMG ducts were ventrally exposed and cut. Saliva was collected in pre-weighed Eppendorfs as seen in Fig. 1E. Saliva collection proceeded for 5 min following stimulation with pilocarpine (0.5mg/kg i.p.). The volume of saliva was calculated as 1mg = 1µl saliva and results were expressed as µl saliva/min.

Depletion of LY6G/LY6C expressing cells

For inflammatory cell depletion, 200 µg/mouse of Ly-6G (Gr-1), Clone RB6-8C5 (eBioscience, 16-5931) was i.p.-administered, 24 hrs prior to poly (I:C) local injection. Saliva was collected and tissues were harvested 24 hrs post ductal infusion.

Histopathologic examination

Harvested SMGs were fixed in 10% neutral buffer formalin, processed and embedded in paraffin for long term storage. Poly (I:C) induced histomorphologic changes and immune cell infiltration were examined using conventional H&E stain and contrasted versus the saline injected control glands.

Immunohistochemical analysis

Three µm tissue sections were deparaffinized, rehydrated, and unmasked in a single step using Trilogy™ (Cell Marque, Rocklin, CA, 920P-06). Sections were incubated in 3% hydrogen peroxide solution for 20-30 minutes, and 1% BSA in 1X TBS, pH 7.6 for 5 minutes. Tissue sections were then incubated at 4°C overnight, with the rabbit polyclonal antibodies against: MPO (1:1000, catalog number PB9057; BosterBio, USA), NKCC1 (1:6000, catalog number ab59791; Abcam Ltd), TMEM16A (ready to use, catalog number ab53213; Abcam Ltd), M3R (1:1000, catalog number sc-9108; Santa Cruz Biotechnology), ZO-1(1:1000, catalog number ab191143; Abcam

Ltd), laminin (1:250, catalog number L9393; Sigma-Aldrich) or the goat polyclonal antibody AQP-5 (1:1000, catalog number sc-9890; Santa Cruz Biotechnology), followed by 1 hr incubation with the Dako goat anti-rabbit (1:200, catalog number P0448), donkey anti-rabbit, alexa fluor 488 for the M3R detection (1:1000, catalog number 21206) or rabbit anti-goat for AQP-5 detection (1:200, catalog number P0160) horseradish peroxidase. Colour was developed for 5 mins in DAB solution (Pierce™ 34002) and slides were counterstained in Mayer haematoxylin and DPX-mounted for light microscopy.

RT-qPCR analysis

For total RNA extraction RNeasy® Micro Kit (74004, Qiagen) was used. iScript™ cDNA Synthesis kit (170-8890, Bio-Rad) was used to reverse transcribe 100 ng of extracted RNA. PCR reactions (10 µl/well) were prepared by adding SsoAdvanced ™ Universal SYBR Green Supermix (172-5271, Bio-Rad), primers (PrimerDesign™, Ltd.: AQP-5 NM_009701.4, NKCC1 (Slc12a2) NM_009194.3, TMEM16A NM_178642.5, M3R NM_033269.4, HPRT (Hypoxanthine guanine phosphoribosyl transferase) NM_013556 and cDNA template. Thermal cycling was performed using Corbett RotorGene 6000 System (Qiagen, UK). In all RT-qPCR experiments, relative gene quantification was assessed according to the following equation: $\Delta\Delta CT$= [Ct GOI Exp – Ct HKG Exp] - [Ct GOI Cal – Ct HKG Cal]: Ct: cycle threshold, GOI: gene of interest, Exp: poly (I:C)-injected glands, HKG: housekeeping gene showing the highest stability (HPRT (Hypoxanthine guanine phosphoribosyl transferase)), Cal: control glands injected by the vehicle. There were three biological replicates for each experiment and the values were analysed by GraphPad Prism Version 5.01 (GraphPad software, USA).

Flow cytometry

Single SMG cells were blocked with TruStain fcX™ anti-mouse CD16/32 antibody (101319, Biolegend) and stained with the Biolegend fluorochromes: FITC-F4/80 (catalog number 123107) , PE-CD45 (catalog number 103207), PE/CY7-CD11b (catalog number 101215), APC- LY6G (catalog number 127613) and APC/CY7- LY6C (catalog number 128025) at 4°C for 1 h. Cells were then washed with 100 µl of cell staining buffer and compensations for spill over and spectral overlap were established by OneComp eBeads® (01-1111-41, eBioscience, Ltd, UK). Cells were analysed with a FACSCalibur CantoII, and data was analysed using the free online Flowing Software 2.5.1.

Statistical analysis

Results were shown as mean ± SEM (standard error of means). Statistical significance between individual comparisons was determined using Student t-test. The calculations were performed with the statistical software package GraphPad Prism (version 7). P values ≤ 0.05 were considered statistically significant.

Results

Single poly (I:C) dose induced rapid loss of function

Mean flow rate of pilocarpine-stimulated saliva was measured from the vehicle-injected control and poly (I:C)-infected glands, at 6 hrs, 9 hrs or 24 hrs following poly (I:C) retrograde injection. No difference in mean flow rates was recorded between the vehicle injected glands and un-injected normal SMGs ($p>0.05$). Conversely, the poly (I:C) injected glands exhibited rapid and extremely significant ($p<0.0001$) loss of function (Fig. 2).

Intraepithelial invasion of MPO-positive immune cells

Sections from the control and poly (I:C)-injected glands, at various experimental time points, were stained with H&E. Besides, MPO, which is expressed in lysosomes of monocytes as well as azurophilic granules of neutrophils[12] was used to mark the acute infiltrating cells. Normal SMGs showed compact lobular structure with packed acini and patent ductal system. Six hours post poly (I:C) inoculation, the SMG vasculature exhibited margination and transmigration of acute inflammatory cells. Surprisingly, the inflammatory cells were seen invading the duct lining, pushing and flattening the native duct epithelial cells, with frequent extrusion into the duct lumens. Similarly, inflammatory cells were frequently seen invading and occupying acinar cells adjacent to blood vessels. By 9 hrs, widespread infiltration of immune cells was displayed in extended stromal spaces, obscuring interlobular ducts and invading inter-acinar tissues. Likewise, after 24 hours of poly (I:C) injection, some infrequent vacuolar degeneration and interlobular oedema transformed vast parts of the gland into an island-like appearance. Moreover, diffuse inflammatory cell infiltrate was seen throughout the whole glandular tissues, with the predominant cells exhibiting the multilobulated, doughnut-shaped nucleus which characterizes active neutrophils. After 6 hrs of introducing poly (I:C), MPO-positive cells were clustered in the peri-vascular and peri-ductal vicinities. By 9 hrs, more extensive interlobular MPO positivity was perceived and the immune cells were seen within the gland acini and ducts. After twenty-four hours, MPO positive cells were ubiquitously detected in interlobular, inter-acinar and more interestingly intra-acinar locations, analogous to the H&E intrusive patterns (Fig. 3).

Poly (I:C) mediated functional compromise independent of immune cell infiltration

Immunohistochemistry substantiated abundant MPO-positive cellular infiltrate in response to poly (I:C) local introduction. Accordingly, we hypothesized that these cells may be major contributors in the poly (I:C)-mediated SMG injury and hypofunction. To validate our theory, we used the RB6-8C5 monoclonal antibody which binds to neutrophils [13] and monocytes [14]. Intraperitoneal injection of 200 μg of RB6-8C5 was administered into the mice, 24 hrs before poly (I:C) local injection, and saliva was collected 24 hrs after infection. Successful depletion of the acute inflammatory cell infiltrate was reflected in the flow cytometry results, which showed that the $CD45^+$ fraction was declined from 21.47% in the poly (I:C) injected SMGs, to 8.62% in the poly (I:C)-infected glands from mice primed with the depletion antibody. Moreover, gating the $CD45^+$ cells within the $F4/80^-$ $CD11b^+$ channel, revealed that the Rb6-8C5 depletion drug efficiently reduced the $LY6G^+/LY6C^+$ populations (Fig. 4A). To explore if RB6-8C5 had efficiently depleted the MPO-positive immune cell populations in the SMGs, immunohistochemistry was conducted which showed that the Rb6-8C5 antibody successfully repressed MPO expression in the SMGs (Fig. 4B). Depletion of the MPO-positive inflammatory cells, 24 hrs prior to poly (I:C)

retrograde duct injection did not induce any recovery in the SMG function (Fig. 4C), which ruled out the role of these aggressively infiltrating cells in the poly (I:C)-induced loss of function.

Poly (I:C) mediated transcriptional downregulation and disrupted localization of key water-driving molecules

Next, we aimed at investigating the integrity of key water-driving molecules in the salivary glands: M3R, AQP5, NKCC1 and TMEM16A. RT-qPCR revealed an extremely significant downregulation (approximately 80% of the baseline level) in the mRNA expression levels of all tested genes (Fig. 5). In addition, immunoperoxidase labelling of SMGs revealed that following poly (I:C) retrograde infusion, a remarkable reduction was seen in all key water driving molecules. In addition, a markedly disrupted and altered immunolocalization of these molecules was displayed in the form of punctate, beaded and shrunken acinar cytoplasmic granules and thick patches (Fig. 5).

Aberrant expression of laminin and ZO-1 in the acutely injured SMGs

TJs together with the BM, seal the intercellular space and establish apical polarity by providing physical segregation between the basolateral and apical domains of the cell membrane [15]. Since intact salivary gland functioning relies on this integral polarization, we investigated the expression of ZO-1, as a marker of TJ integrity [16] and laminin, as a predominant component of the BM [17]. Immunolabelling verified the evident loss, shrinkage and wriggling of the smooth apical ZO-1 outline, following innate immune activation (Fig. 6). While the basement membrane pan laminin marker displayed a uniform delineation of normal glandular epithelial cells, the poly (I:C)-injected glands exhibited a distinctively irregular laminin immunostaining. Disruptions ranged from thick, shadow-like expression to vacuolated, soap bubble-like patterns (Fig. 6).

Discussion

Salivary glands respond to a wide array of insults by reduction in secretion or hyposalivation. In the present research, we introduced a novel acute salivary gland injury model, that can be constantly and reliably reproduced. By developing this model, we aimed at characterizing the acute: functional, inflammatory and tissue changes, sequential to local exposure of the SMG epithelial cells to a potent innate immune stimulant: poly (I:C). The SMGs in the current model, displayed a rapidly progressive functional decline, until the SMGs ceased secretion completely after 24 hrs. Previous studies demonstrated that multiple, systemic injections of poly (I:C) into Sjögren's syndrome-prone, NZB/WF1 mice, resulted in loss of glandular function [10, 11]. The model presented herein, is unique in demonstrating the direct influence of innate immune activation on the SG tissues and functional responses, ruling out possible extraneous impacts arising either from systemic delivery or autoimmune susceptibility of mice.

Poly (I:C) induced widespread infiltration of inflammatory cells having the histologic features of active neutrophils (bilobed nuclei). Surprisingly, a unique pattern of intra-acinar and intra-ductal invasive distribution was displayed by these cells. They were frequently seen dislocating and flattening the resident duct nuclei, in addition to being commonly extruded into the lumens. Interestingly, duct cells as well as acinar cells [18] have demonstrated ability to respond to inflammatory signals by the production of chemokines. Accordingly, the inherent ability of the salivary gland epithelial cells to produce these low molecular weight chemo-attractants, may have guided the infiltrating immune cells to the perceived intra-epithelial invasive positions.

Immunolabelling the SMG tissues with MPO disclosed that the robustly recruited immune cells, tethering, transmigrating and invading into ducts and acini were MPO positive, which underscored their neutrophil/monocyte identity [12]. The monoclonal RB6-8C5 antibody was shown to bind to Ly6C which is neutrophils, dendritic cells (DCs), subsets of monocytes, macrophages and lymphocytes [13]. In the present study, RB6-8C5 antibody was used to dually deplete neutrophils and monocytes and investigate their injurious role in the acute loss of function. Histopathology, flow cytometry and immunohistochemistry showed that priming of the mice with RB6-8C5 markedly attenuated immune cell invasion into the SMGs, after 24 hrs of poly (I:C) treatment. Surprisingly, treatment of mice with the anti-Ly6G/Ly6C, did not induce functional recovery. These experiments verified that innate immune activation interferes with the secretory ability of the SMGs, independent of the invasive immune cell signal. Findings from the current experiments, combined to other studies which demonstrated irrelevance between secretory hypofunction and immune cellular infiltration [19], strongly implicate an alternative impairment mechanism by which the SG epithelial cells endogenously respond to injury and cease secretion.

The duct ligation model has been used by many groups to induce organ dysfunctions, based on inflammation and fibrosis, which take place due to obstructing the fluid pathway [20]. Rapid loss of function perceived in the innate immune model presented herein, paralleled loss and aberrant cytoplasmic expression of the membranous: muscarinic receptor M3R, AQP5 water channel, ion transport molecules NKCC1 and TMEM16A. To appreciate the crucial role played by the assessed water and ion transport molecules, it is essential to note that inhibition of NKCC1 [21], TMEM16A [22] and AQP5 [23], severely compromised or interfered with the SG ability to secrete.

One significant statement arising from this model, is the importance of the consistent membranous localization of these transport proteins in sustaining normal glandular functions. As far as our knowledge extends, the salivary gland injury model presented herein, is the first in vivo demonstration of the immediate disruption of key water and ion transport molecules at the gene and immunolocalization levels, in response to innate immune activation. Future experiments will aim at substantiating the mechanism(s) underlying the dual transcriptional downregulation and disrupted dispatch of the key water and ion transport molecules, perceived in the current model.

Basement membranes act as platforms for epithelial cell adhesion, to provide structural support, to divide tissues into compartments, and to regulate cell behaviour including polarity [24]. Previous studies demonstrated a fundamental shift in plasma membrane traffic toward intracellular compartments, when epithelial cells lose their cell polarity [25]. The island-like morphology of the SMG after poly (I:C) injection, added to the disrupted expression of the ubiquitous BM protein; laminin, may account for the aberrant, granular, cytoplasmic expression of the predominantly-membranous water and ion transport proteins and suggest potential loss of polarity and orientation abilities of these secretory epithelial cells, as a mechanism for the inapt delivery of the apically expressed proteins.

By means of regulating transport of fluid and solutes, as well as retaining the apico-basal epithelial polarity [26], TJs play an important role in saliva secretion. ZO-1, which forms a bridge between the TJ strands and the actin cytoskeleton, has been recognized as a marker for the integrity of tight junctions[16]. In the control SMG acinar and duct cells a strong, 'chicken-wire' pattern of staining was displayed on apico-membranous surfaces. Following innate immune injury, ZO-1 revealed a discontinuous, haphazardly oriented, shrunken or lost ZO-1 immunoexpression on apical membranes. The current model featuring dysfunction and aberrant TJ expression in the salivary glands, may enhance the understanding of the role played by this key molecule not only in paracellular water secretion but also in trafficking and signalling of protein complexes.

Thorough and comprehensive investigation of the mechanism(s) underlying the innate immune-mediated SMG dysfunction, utilizing the current acute injury model, will elucidate many of the unrecognized signals and trafficking defects that may be generally involved in SG impairment of secretion. Novel therapeutic targets can be uncovered, to terminate the progressive loss of salivary gland function associated with the most common chronic and autoimmune salivary gland diseases such as Sjögren's syndrome.

Acknowledgements

We acknowledge Dr. Maria Jose Martinez Bravo (mucosal & salivary biology division, King's College London) for her support with the flow cytometry experiments and Mr. Carl Hobbs (Wolfson centre for age-related diseases, King's College London) for the technical assistance with pan laminin staining.

Conflict of interest Statement

All authors declare that there is no conflict of interest.

References

1. Proctor GB. The physiology of salivary secretion. *Periodontol 2000.* 2016;70:11-25.

2. Lever AR, Park H, Mulhern TJ, et al. Comprehensive evaluation of poly(I:C) induced inflammatory response in an airway epithelial model. *Physiol Rep.* 2015;3.

3. Kanaya K, Kondo K, Suzukawa K, et al. Innate immune responses and neuroepithelial degeneration and regeneration in the mouse olfactory mucosa induced by intranasal administration of Poly(I:C). *Cell Tissue Res.* 2014;357:279-299.

4. Dawson LJ, Fox PC, Smith PM. Sjogrens syndrome--the non-apoptotic model of glandular hypofunction. *Rheumatology (Oxford).* 2006;45:792-798.

5. Proctor GB. Muscarinic receptors and salivary secretion. *J Appl Physiol (1985).* Vol 100. United States2006:1103-1104.

6. Arreola J, Melvin JE, Begenisich T. Activation of calcium-dependent chloride channels in rat parotid acinar cells. *J Gen Physiol.* 1996;108:35-47.

7. Zeng W, Lee MG, Muallem S. Membrane-specific regulation of Cl- channels by purinergic receptors in rat submandibular gland acinar and duct cells. *J Biol Chem.* 1997;272:32956-32965.

8. Zhang GH, Wu LL, Yu GY. Tight junctions and paracellular fluid and ion transport in salivary glands. *Chin J Dent Res.* 2013;16:13-46.

9. Lee MG, Ohana E, Park HW, Yang D, Muallem S. Molecular mechanism of pancreatic and salivary gland fluid and HCO3 secretion. *Physiol Rev.* 2012;92:39-74.

10. Deshmukh US, Nandula SR, Thimmalapura PR, Scindia YM, Bagavant H. Activation of innate immune responses through Toll-like receptor 3 causes a rapid loss of salivary gland function. *J Oral Pathol Med.* 2009;38:42-47.

11. Nandula SR, Dey P, Corbin KL, Nunemaker CS, Bagavant H, Deshmukh US. Salivary gland hypofunction induced by activation of innate immunity is dependent on type I interferon signaling. *J Oral Pathol Med.* 2013;42:66-72.

12. Klebanoff SJ. Myeloperoxidase: friend and foe. *J Leukoc Biol.* 2005;77:598-625.

13. Hickey MJ. Has Ly6G finally found a job? *Blood.* 2012;120:1352-1353.

14. Jutila MA, Kroese FG, Jutila KL, et al. Ly-6C is a monocyte/macrophage and endothelial cell differentiation antigen regulated by interferon-gamma. *Eur J Immunol.* 1988;18:1819-1826.

15. Plachot C, Chaboub LS, Adissu HA, et al. Factors necessary to produce basoapical polarity in human glandular epithelium formed in conventional and high-throughput three-dimensional culture: example of the breast epithelium. *BMC Biology.* 2009;7:77.

16. Hurd TW, Gao L, Roh MH, Macara IG, Margolis B. Direct interaction of two polarity complexes implicated in epithelial tight junction assembly. *Nat Cell Biol.* 2003;5:137-142.

17. Hohenester E, Yurchenco PD. Laminins in basement membrane assembly. *Cell Adhesion & Migration.* 2013;7:56-63.

18. Dios ID. Inflammatory role of the acinar cells during acute pancreatitis. *World J Gastrointest Pharmacol Ther.* 2010;1:15-20.

19. Correia PN, Carpenter GH, Paterson KL, Proctor GB. Inducible nitric oxide synthase increases secretion from inflamed salivary glands. *Rheumatology (Oxford).* 2010;49:48-56.

20. Osailan SM, Proctor GB, McGurk M, Paterson KL. Intraoral duct ligation without inclusion of the parasympathetic nerve supply induces rat submandibular gland atrophy. *Int J Exp Pathol.* 2006;87:41-48.

21. Evans RL, Park K, Turner RJ, et al. Severe impairment of salivation in Na+/K+/2Cl- cotransporter (NKCC1)-deficient mice. *J Biol Chem.* 2000;275:26720-26726.

22. Catalán MA, Kondo Y, Peña-Munzenmayer G, et al. A fluid secretion pathway unmasked by acinar-specific Tmem16A gene ablation in the adult mouse salivary gland. *Proceedings of the National Academy of Sciences of the United States of America.* 2015;112:2263-2268.

23. Krane CM, Melvin JE, Nguyen HV, et al. Salivary acinar cells from aquaporin 5-deficient mice have decreased membrane water permeability and altered cell volume regulation. *J Biol Chem.* 2001;276:23413-23420.

24. Varshney S, Hunter DD, Brunken WJ. Extracellular Matrix Components Regulate Cellular Polarity and Tissue Structure in the Developing and Mature Retina. *Journal of Ophthalmic & Vision Research.* 2015;10:329-339.

25. Low SH, Miura M, Roche PA, Valdez AC, Mostov KE, Weimbs T. Intracellular Redirection of Plasma Membrane Trafficking after Loss of Epithelial Cell Polarity. *Molecular Biology of the Cell.* 2000;11:3045-3060.

26. Baker OJ. Current trends in salivary gland tight junctions. *Tissue Barriers.* 2016;4:e1162348.

Figure Legends:

Fig. 1: Development of the Poly (I:C) injury model in the SMGs

A: Polyinosinic–polycytidylic acid sodium salt (poly (I:C)) diluted in saline and Trypan blue was loaded into a 0.3 ml syringe prior to injection. B: A glass cannula fitted into a polyethylene tube and the poly (I:C)-loaded syringe, was inserted into the sublingual papilla of Wharton's duct. C and D: specific infusion of poly (I:C) into the left submandibular glands (LSMG), escaping the right (R)SMG and the sublingual gland (SLG). E: Extraoral saliva collection was performed by as explained in the text.

Fig. 2: Salivary Flow rates in Control and Poly (I:C)-Injected SMGs

Scatter plot analysis of the mean ± SEM SMG flow rates after 6 hrs, 9 hrs or 24 hrs of poly (I:C) intraductal injection, all compared to the vehicle injected glands (V-C). Non-injected SMGs (C-UN) were compared to the vehicle injected ones to assess the impact of retrograde injection on the gland functional capabilities, and a non-significant change was seen between the two groups. Conversely, poly (I:C) induced an extremely significant reduction in mean flow rates as early as 6 hrs of its infusion and ultimately lead to complete impairment of the SMG function after 24 hrs. ****: $P<0.0001$, NS: non-significant $p>0.05$.

Fig. 3: H&E and MPO Immunostain of control and poly (I:C)-injected SMGs.

A: histomorphology of normal un-injected SMG and B: vehicle injected control SMG. C: Negative MPO expression in the vehicle injected control SMG. D: 6 hrs post poly (I:C) showing apparently preserved histomorphology, with inflammatory cells extruded into duct lumens. E: higher magnification of D revealing margination and transmigration (arrow) of inflammatory cells. F: the peri-ductal and sporadic inter-acinar cells are MPO-positive. G: Another higher magnification photomicrograph showing invasion of the infiltrating inflammatory cells into the SMG duct lining from all directions where blood vessels are sited, note the apparent replacement of native duct epithelial cells (now pushed and flattened, (arrows)) by the plethora of infiltrating cells. H: Extensive infiltration of stromal acute inflammatory cells, 9 hrs after poly (I:C) injection. I: MPO-positive cells invading ducts and interlobular spaces, 9 hrs after poly (I:C). J: 24 hrs following poly (I:C): edema and widening of the interlobular and inter-acinar spaces transforming the gland architecture into island-like morphology, with diffuse inflammatory cell infiltrate broadly occupying the expanded spaces. K: cells exhibiting the histologic features of neutrophils (doughnut-shaped /multilobulated nuclei) can be seen interlobular, inter-acinar and intra-acinar (arrow). L: intra-acinar (red arrow) and intra-ductal (black arrow) MPO-positive cells, 24 hrs after poly (I:C). Original Magnification A and B =16X. C, D, F, H, L=25X. E, G, I, J, K, =40X.

Fig. 4: A: Representative flow cytometry analysis images of RB6-8C5 treated and non-treated glands.

For neutrophil discrimination, cells were serially gated in the CD45+F4/80-CD11b+LY6C+LY6G+ channels. Obvious decline in the percentage of CD45+ cells was perceived in the depleted animals. Note the absence of distinct immune cell populations in the SMGs from mice which were exposed to the depletion drug in contrast to the very characteristic CD45+F4/80-CD11b+LY6C+LY6G populations seen 24 hrs post poly (I:C) injection.

B: RB6-8C5 depleted MPO-positive cells. Representative photomicrographs of SMG tissue sections injected only with poly (I:C) (a&c) and with the Rb6-8C5 depletion antibody followed by poly (I:C) (b&d). Note the depletion

effect conveyed by RB6-8C5 on the MPO signal in the infected SMGs. Original magnification: a, b=10X, c, d=25X.

Fig. 5: Right: mRNA expression of genes encoding water driving molecules; M3R, AQP5, NKCC1 and TMEM16A.

SMGs of mice treated or not-treated with AG were injected with the vehicle or poly (I:C). SMGs were harvested 24 hrs post the local injections, and tested genes were normalized to HPRT. Poly (I:C) intraductal infusion induced an extremely significant transcriptional downregulation of the mRNA of key water driving molecules. Data represent means ± SEM (n=3). ****P < 0.0001. Left: Representative immunohistochemistry of key water driving molecules; M3R, AQP5, NKCC1 and TMEM16A. Control SMG (V-C) showed: fluorescently immunolabelled M3R displaying a punctate expression pattern in the basal membrane of acini and in the cytoplasm and membrane of epithelial cells lining the intercalated and striated ducts. Positive furrow-like AQP-5 immunostaining on the luminal membranes of acinar cells. Strong basolateral and apical NKCC1 as well as specific duct cell positivity (yellow arrows). TMEM16A immunolabelled acinar apical domains as well as acinar-ductal interconnecting branches. Poly (I:C)-injected glands: 24 hrs post poly (I:C) SMGs displayed remarkably reduced M3R expression compared to the control glands. AQP-5 was seen in the form of thickened membrane patches (green arrows), basolateral staining (red arrows) as well as granular cytoplasmic immunostaining (black arrows). NKCC1 revealed an irregular intense, granular cytoplasmic expression. TMEM16A expression showed reduced and altered positive cytoplasmic granularity.

Fig 6: Immunolocalization of laminin and ZO-1 following poly (I:C) introduction.

Pan Laminin uniformly immunolabelled the membranous domains of normal ductal and acinar cells. After poly (I:C), thickened, shadow-like, vacuolated and soap-bubble, irregular immunostain was perceived. (Original Magnification = 25x). ZO-1 displayed speckled or uniform linear membranous expression of acini and ducts. Poly (I:C) induced obvious loss and irregularity of the TJ marker (Original Magnification=40x).

Fig. 1

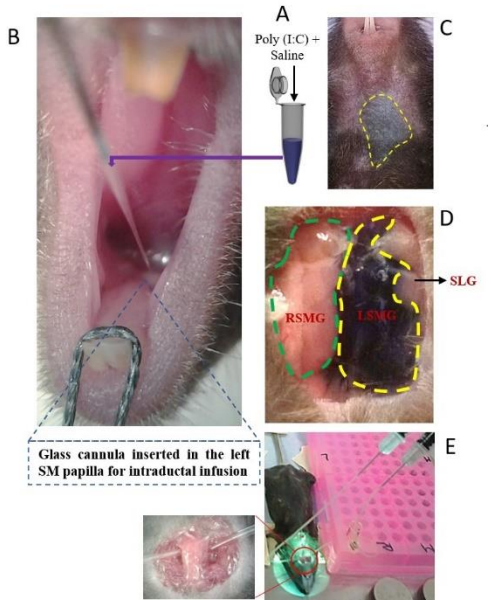
A
Poly (I:C) +
Saline
B
C
D
SLG
RSMG
LSMG
E
Glass cannula inserted in the left
SM papilla for intraductal infusion

Fig. 2

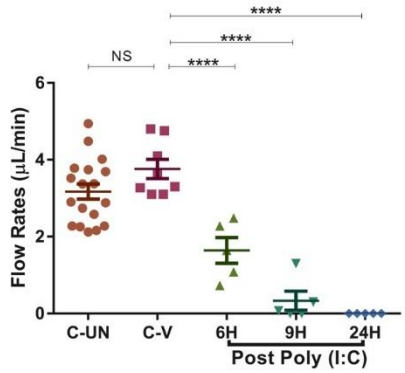
****
****
NS
****
Flow Rates (µL/min)
6
4
2
0
C-UN
C-V
6H
9H
24H
Post Poly (I:C)

Fig. 3

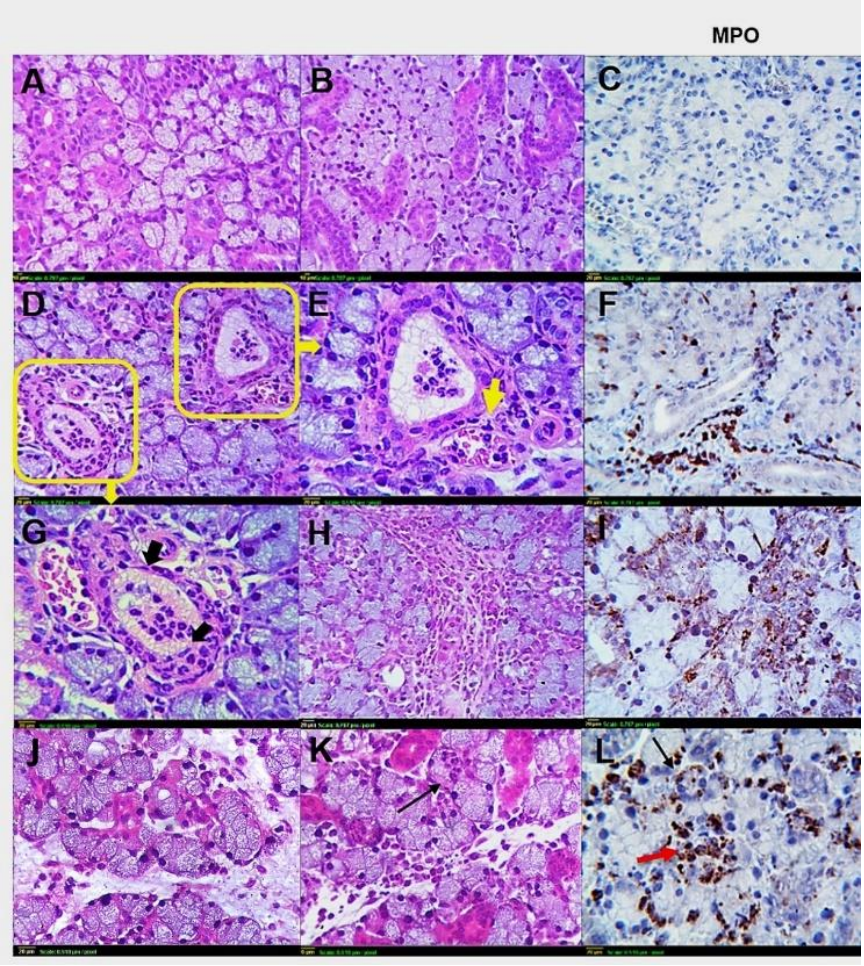

Fig. 4.

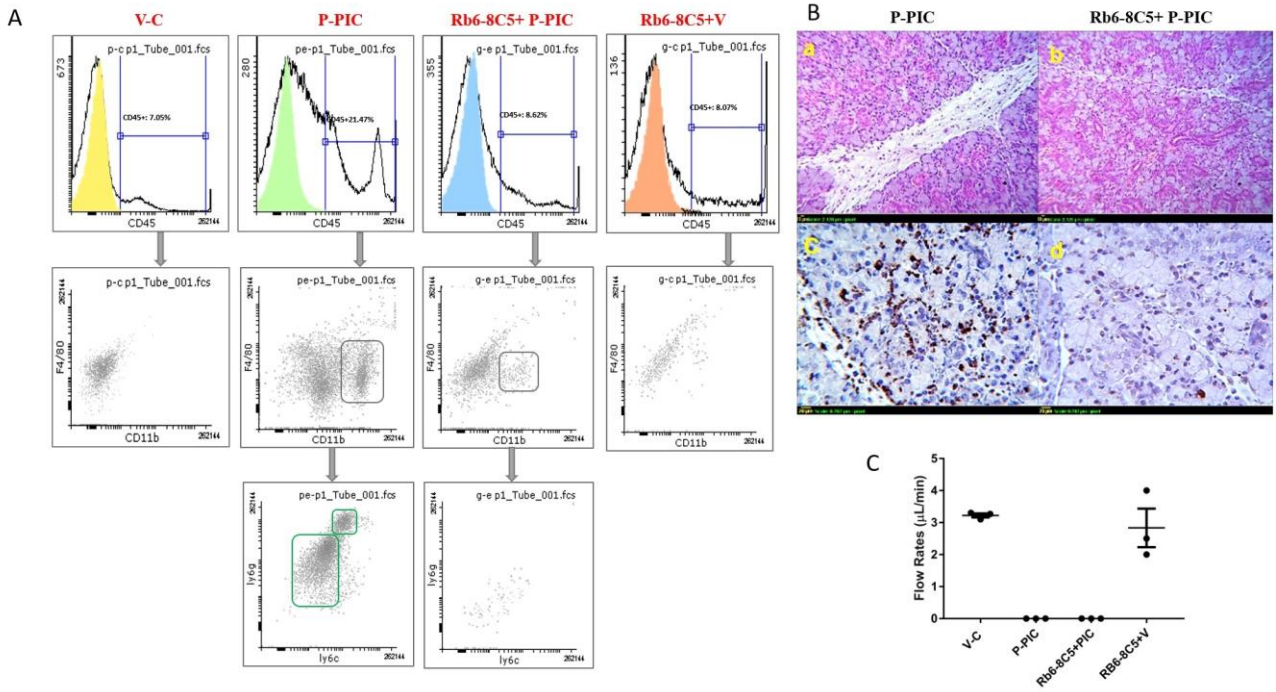
A
V-C
P-PIC
Rb6-8C5+ P-PIC
Rb6-8C5+V
CD45
CD11b
F4/80
ly6g
ly6c
B
P-PIC
Rb6-8C5+ P-PIC
a
b
c
d
C
Flow Rates (μL/min)
V-C
P-PIC
Rb6-8C5+PIC
RB6-8C5+V

Fig. 5.

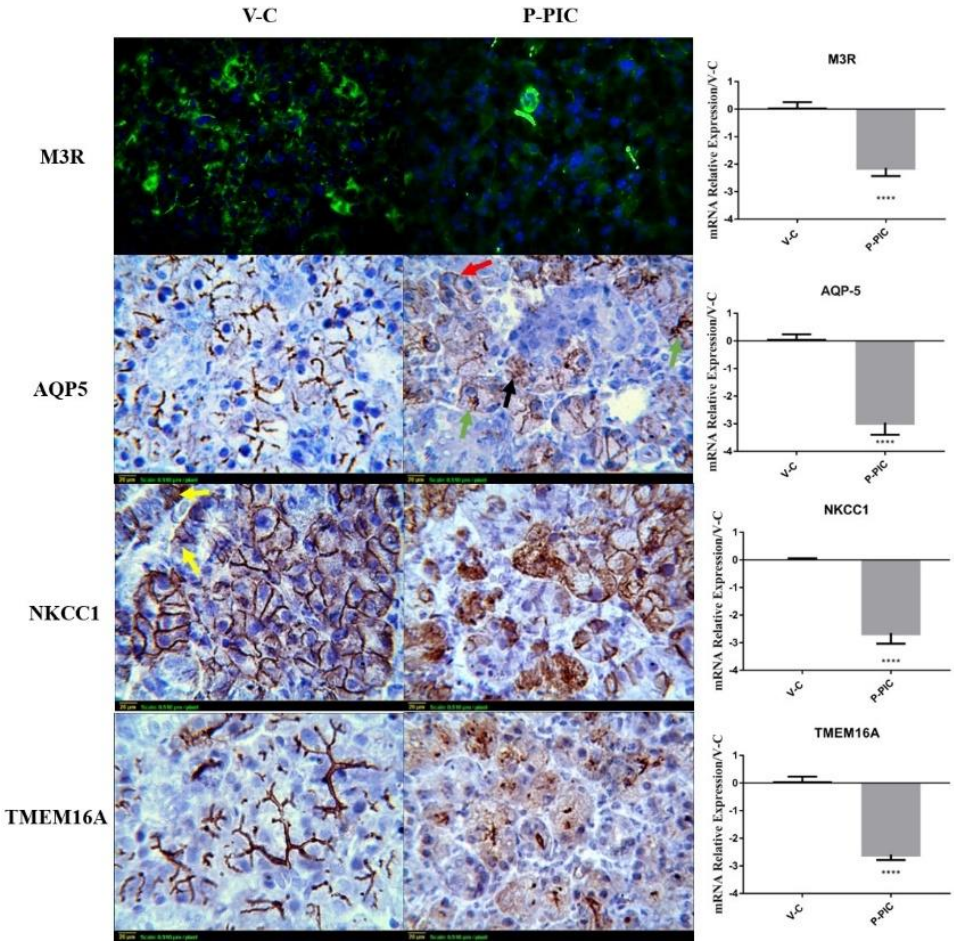
V-C
P-PIC
M3R
AQP5
NKCC1
TMEM16A
mRNA Relative Expression/V-C
V-C
P-PIC

Fig. 6.